water

MDPI

Article

Assessing Spatial Variability and Trends of Droughts in Eastern Algeria Using SPI, RDI, PDSI, and MedPDSI—A Novel Drought Index Using the FAO56 Evapotranspiration Method

Abdelaaziz Merabti [1], Hanaa Darouich [2], Paula Paredes [2], Mohamed Meddi [3] and Luis Santos Pereira [2,*]

[1] Laboratoire de Préservation et Protection des Ressources en Eau, Département des Sciences de l'eau et Environnement, Université Blida 1, Blida 09000, Algeria
[2] LEAF-Landscape, Environment, Agriculture and Food, Associated Laboratory TERRA, Instituto Superior de Agronomia, Universidade de Lisboa, 1349-017 Lisbon, Portugal
[3] Laboratoire GEE, Ecole Nationale Supérieure d'Hydraulique de Blida, Blida 09000, Algeria
* Correspondence: luis.santospereira@gmail.com

Abstract: Drought is one of the most severe natural disasters worldwide, but with a particular emphasis in sub-humid and semi-arid climates. Several indices have been created to appropriately identify drought's characteristics and variability. The main objectives of this study consisted of analyzing the behavior of different indices applied in northeast Algeria and comparing them across a long-term data set (1961–2014). The SPI and RDI at 9-month time scales were compared to the PDSI and MedPDSI based on 123 rainfall stations and gridded PET data interpolated to all the locations. A principal component analysis (PCA) in S-mode with varimax rotation (RPC) was applied to the monthly values of all indices to analyze the spatiotemporal patterns of droughts. Two principal components were retained, which identified two sub-regions with coherent differences related to their distance from the Mediterranean Sea and the UNEP aridity index. Trends in the RPC scores were assessed using the modified Mann–Kendall (MMK) test and Sen's slope estimator, which showed a fundamental difference between the two sub-regions. The RPC of all drought indices showed trends of decreases in the frequency and severity of droughts in the northern sub-region, and trends of increases in the frequency and severity of droughts in the southern region, where the climate is mostly semi-arid and arid. Only a few cases were statistically significant, mostly when using the PDSI and MedPDSI for the southern sub-region. The spatial patterns of moderate, severe, and extreme drought occurrences were similar for the SPI and RDI pair of indices based on the probability of rainfall anomalies, and for the Sc-PDSI and MedPDSI pair based on water balance anomalies. The interpretation of the spatial variability of droughts, mainly of the extreme ones, was supported by an analysis of semi-variograms. The novel index MedPDSI compared well with the other indices and showed advantages of performing the soil water balance following the FAO56 dual K_c method with the actual olive evapotranspiration instead of PET, and of better explaining the spatial variability of extreme droughts; in addition, the trends detected were significant for both the northern and southern sub-regions.

Keywords: drought patterns; trends; PDSI; MedPDSI; SPI; RDI; Algeria

Citation: Merabti, A.; Darouich, H.; Paredes, P.; Meddi, M.; Pereira, L.S. Assessing Spatial Variability and Trends of Droughts in Eastern Algeria Using SPI, RDI, PDSI, and MedPDSI—A Novel Drought Index Using the FAO56 Evapotranspiration Method. *Water* **2023**, *15*, 626. https://doi.org/10.3390/w15040626

Academic Editors: Athanasios Loukas and Leonardo V. Noto

Received: 29 December 2022
Revised: 15 January 2023
Accepted: 1 February 2023
Published: 5 February 2023

1. Introduction

Droughts are extreme phenomena of natural origin consisting of persistent lower-than-average precipitation of uncertain frequency, duration, and severity, the occurrence of which is unpredictable or difficult to predict, resulting in diminished water resource availability and a diminished carrying capacity of ecosystems [1]. A drought affects the runoff of natural rivers and surface and underground reservoirs, causing agricultural, hydrological, and socio-economic impacts on a range of spatial and temporal scales [2]. It is of utmost importance to identify drought behavior and variability with the best accuracy,

especially in drought-prone countries and regions [3], particularly where rainfed agriculture is vulnerable, as in Algeria [4].

Many drought studies have been conducted across the Mediterranean region, including ones performed for Algeria [5] using the standard precipitation index (SPI, McKee et al. [6]) and the drought reconnaissance index (RDI, Tsakiris et al. [7]). The use of both indices provided very good responses, but further assessments are required for more assertive conclusions because droughts are complex phenomena and their complexity is currently increasing with climate change [8]. Hoerling et al. [9] and Tramblay et al. [4] reported an increased frequency and severity of droughts, with the latter authors considering various future climate change scenarios. Previously, Giorgi and Lionello [10] pointed out that the Mediterranean basin is extremely vulnerable to climate change, with increasing temperatures and decreasing precipitation. Sousa et al. [11] identified the North Atlantic oscillation (NAO) index as being related to drought in a large part of the Mediterranean region and Moreira et al. [12] reported that the SPI drought class predictions in Portugal were driven by the NAO index, while Hallouz et al. [13] identified the NAO and the Mediterranean oscillation (MO) indices in relation to drought in the Northwest of Algeria. A significant increase in drought occurrence in the region was reported by Spinoni et al. [14], and significant trends of drier conditions over the Mediterranean region have been reported in various studies [11,15]. However, other researchers have not found significant trends [5,16–18]. This non-agreement points out the complexity of drought phenomena [19,20]. Nevertheless, the likely increase in dryness impacts the agricultural sector, particularly rainfed crops such as wheat and olive trees [21,22]. A better understanding of drought behavior and characteristics is essential for base crop and water management aimed at mitigating the negative impacts of droughts, particularly through a prediction and warning system [1,8,23].

Several drought and rainfall studies focused in northern Algeria, mostly relative to the northwestern areas, have reported a significant decrease in precipitation, larger than in northeastern Algeria [5,24–27]. Meddi et al. [28] identified multiple factors that likely influence rainfall variability, namely longitude, the distance from the Mediterranean Sea, and topography. Habibi et al. [29] studied the probability of drought occurrence using the SPI and Markov chains in the Chéliff–Zahrez basin, while Habibi and Meddi [30] used the SPI and geographic information systems to map the spatial variability of droughts.

Several indices have been created and employed to appropriately identify and analyze drought's characteristics, namely: severity, intensity, duration, and spatial extent [3,31]. The Palmer drought severity index (PDSI, Palmer [32]), based on a soil water balance equation using potential evapotranspiration (PET, Thornthwaite [33]), is very commonly used in drought monitoring. The SPI requires only monthly precipitation data and, like the RDI, has been used worldwide and in a previous study [5,27]. The standardized precipitation evapotranspiration index (SPEI, Vicente-Serrano et al. [31]) includes precipitation (P) and PET estimated from PM-FAO ET_o. Several other indices have been suggested and used, e.g., the percent of normal precipitation index (PNPI; Willeke et al. [34]); the streamflow drought index (SDI; Nalbantis and Tsakiris [35]); the China-Z index (CZI); the modified China-Z index (MCZI) [36,37]; and the effective drought index (EDI; Byun and Wilhite [38]), the authors of which reported on its limited utility in different climatological zones other than the one where it was developed (e.g., Ogunrinde et al. [39]). Previously, Wells et al. [40] contributed to solving those spatial difficulties by developing the self-calibrated PDSI (Sc-PDSI), which considers some climatic information of the study area. Based on this Sc concept, Pereira et al. [41] suggested a modification of the soil water balance adopted in the PDSI by replacing the use of the PET by the actual ET of an olive crop. This index, the MedPDSI, was proposed for the Mediterranean climate regions. Its application and testing were reported by Paulo et al. [42] and it could be considered superior to the PDSI for a wide application in Portugal. Moreover, the MedPDSI, like the PDSI, compared well with the SPI and RDI computed for a 9-month time scale, i.e., the SPI-9 and RDI-9.

This study, considering the above review and previous results for Portugal and Algeria, aims to: (a) improve the knowledge on drought time variability and trends, as well as the spatial variability in northeastern Algeria for the period from 1961 to 2014; (b) assess

the behavior of various drought indices—SPI-9, RDI-9, ScPDSI, and MedPDSI—when comparing them from the perspective of spatiotemporal evolution and trend detection; (c) use semi-variograms to better assess the space variability of droughts; and, in particular, (d) test the novel MedPDSI for the varied Mediterranean climate of Algeria. Therefore, this study is innovative in terms of considering and testing a novel drought index in relation to other well-proven drought indices to assess the time and spatial variability of droughts, as well as using semi-variogram analyses to confirm space variability. Moreover, the study is expected to provide information relative to water management offices concerned about the development of drought monitoring and early warning systems.

2. Materials and Methods

2.1. Study Area—Northeastern Algeria

The study area extended between the longitudes of 3°15′6″ E and 8°40′10″ E and the latitudes of 37°5′00″ N and 34°32′30″ N (Figure 1). Due to its vast geographical area of about 109,000 km^2 and the diversity of its topography, the Algerian NE is characterized by different climates. The region is bounded to the north by the Mediterranean Sea. The coastal zone receives the most important precipitation of the whole country, reaching 1700 mm year^{-1}. The study area is bounded to the east by the Tunisian border. The annual precipitation decreases towards the inland regions until the Saharian Atlas and the southern plains bordering the Sahara Desert, where the precipitation does not exceed 150 mm year^{-1}.

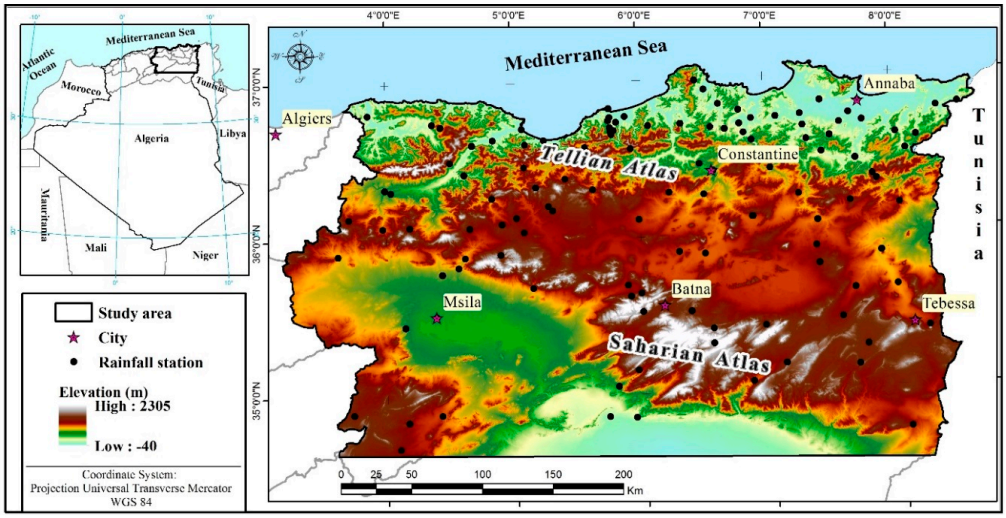

Figure 1. Map of the study area with locations of rainfall stations.

Monthly precipitation data were obtained from the National Hydraulic Resources Agency (ANRH) using 123 rainfall stations relative to the time period of 1960–2014. The stations were chosen based on the length of the time series and their locations, which allowed good coverage of the study area. These data were used in a previous study [27], where the procedures used for completing the time series when the records had less than 10% of missing monthly values are described; otherwise, the station was not considered. The study also explained that the precipitation data were tested for homogeneity using the Wilcoxon sequential test [43] and that non-homogenous precipitation series were corrected with the double and the cumulative residuals methods [44] using the neighboring stations with homogenous data. Ordinary kriging was used for interpolation with consideration of the altitude effects. The annual precipitation data's spatial distribution is presented in Figure 2a, which shows its decrease from north to south, denoting the effect of the Atlas Mountain chain in combination with the general circulation of the atmosphere.

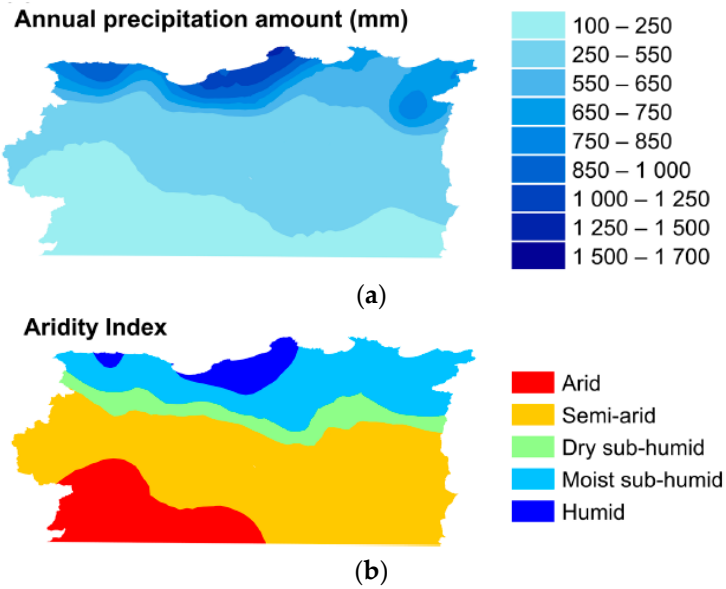

Figure 2. Precipitation and aridity maps of northeastern Algeria: areal distribution of (**a**) precipitation and (**b**) the UNEP aridity index.

The ET_o (or PET) data were obtained from the Climate Research Unit Time Series (CRU-TS v. 4.06) developed at the University of East Anglia, United Kingdom, which consists of a monthly climatic database in a regular grid of 0.5° that spans from 1901 to 2015 [45]. The gridded CRU PET (ET_o) was computed using the FAO56-PM equation [44], but with variables estimated using the absolute values of the monthly average daily temperature, monthly average daily maximum and minimum temperature, vapor pressure, and cloud cover, and from a fixed monthly climatology for wind speed [46]. Cloud cover was used to estimate the number of bright sunshine hours and then to estimate solar radiation, as described by Harris et al. [46], using a procedure that has been validated by near 20 years of use.

The ET_o data employed in the current study cover the same period of the rainfall data (1960–2014). The monthly average daily ET_o data were extracted and interpolated for the point location of the weather stations using an ordinary kriging. This dataset was selected because it is known to have good accuracy: Ahmed et al. [47] used CRU-TS over Pakistan to evaluate the general circulation model for simulating precipitation and temperature; Oduro et al. [48] used CRU-TS with CMIP6 multimodal to study seasonal and annual trends in the near-surface temperature in Ghana; and Pour et al. [49] used the monthly mean temperature and PET data from CRU to study the spatiotemporal aridity and the shift of drylands in Iran.

The aridity index (Figure 2b), which is the average ratio of the long term annual means of precipitation and potential evapotranspiration estimated with the Thornthwaite method [33], increased from the northern to the southern areas, where droughts are associated with natural water scarcity.

2.2. Drought Indices

2.2.1. The Self-Calibrating Palmer Drought Severity Index (Sc-PDSI)

The estimation of the Sc-PDSI is based on the monthly water balance of the original PDSI two-layer soil [32]:

$$P = ET + RO + (R - L) \quad (1)$$

where P is the precipitation, ET is the evapotranspiration, RO is the runoff, R is the soil water recharge, and L is the soil water loss as deep percolation.

The precipitation (P_j) climatically appropriate for the existing conditions represents the amount of precipitation that is expected to maintain a normal soil moisture level in a

single month j, and is computed using the weighting factors α, β, γ, and δ, also called the water-balance coefficients, calculated for each month j as the ratio between the average of the estimation (Equation (1)) and the potential terms over a calibration period, as follows:

$$p_j = \alpha_j PET_j + \beta_j PR_j + \gamma_j PRO_j - \delta_j PL_j \quad (2)$$

The potential terms of runoff (PRO), soil water recharge (PR), and soil water loss (PL) are calculated along their associated variables RO, R, and L, and they rely on the available water-holding capacity of the soil. As previously pointed out, the potential evapotranspiration (PET or ET_o) was estimated using the FAO-PM equation.

The moisture anomaly index (z), which is a standardized measure that shows how wet or dry a single month is without regard to recent precipitation trends, is obtained as follows:

$$z = k_j(P_j - p_j) \quad (3)$$

where k_j is a weighing factor representing the climatic characteristic for the month j, originally derived using the equations above and data from nine different locations in seven USA states [32]. The z index is used to estimate the PDSI for a given month using a general equation:

$$X_j = 0.897X_{j-1} + \left(\frac{1}{3}\right)z_j \quad (4)$$

The resulting PDSI categories are defined in Table 1 [32].

Table 1. Classification of the PDSI value.

PDSI Value	PDSI Category
≥4.00	Extreme wet spell
3.00 to 3.99	Severe wet spell
2.00 to 2.99	Moderate wet spell
1.00 to 1.99	Mild wet spell
0.50 to 0.99	Incipient wet spell
0.49 to −0.49	Normal
−0.50 to −0.99	Incipient drought
−1.00 to −1.99	Mild drought
−2.00 to −2.99	Moderate drought
−3.00 to −3.99	Severe drought
≤−4.00	Extreme drought

The values 0.897 and 1/3 were called the duration factors by Palmer [32]. They were obtained from two locations (in western Kansas and central Iowa) and express the sensitivity of the index to precipitation events. The PDSI values need the computation of three intermediate indices, X_1, X_2, and X_3, using Eq 4. The values of X_1 and X_2 are the severity of a wet or dry spell, respectively, that might become established at the location under study, and X3 is the severity of a wet or dry spell that is currently established.

The Sc-PDSI was developed by Wells et al. [40] and is aimed at removing backtracking, and at creating a subtle transition from dry to wet spells. In this formulation, the empirically derived climatic characteristic (k) and duration factors (0.897 and 1/3) are replaced with values that are based upon the historical climatic data of the study site. The self-calibration procedure initiates after having calculated the moisture departure, which is the difference (Pj–pj) between the actual precipitation in a given month and the precipitation climatically appropriate for the existing environmental condition, and several sequential steps are followed to obtain the self-calibrated PDSI [40].

2.2.2. The Modified PDSI for Mediterranean Regions, MedPDSI

The MedPDSI is a modification of the PDSI by considering the actual ET (ET_a) of a rain-fed olive crop as drought reference crop for the soil water balance (Equation (1))

instead of PET; the olive crop was selected because it is a perennial crop that is well adapted to water stress and to Mediterranean environments [41,42].

In MedPDSI, the soil water balance is calculated using the dual K_c approach [44,50], thus separately computing both ET components, the soil evaporation, and the crop transpiration. The soil water balance can be determined for different soil types. The soils are defined according to their texture and the average soil water-holding characteristics of the soil layers; soil evaporation is assumed to originate from the upper surface layer. The soil water balance considers the rooting depth of a mature olive grove to extract water from the soil, and ET_a varies according to the sensitivity of the olive trees to water stress [42]. The general equation of the soil water balance is:

$$\Delta ASW = P - ET_a - R_{off} - D_p \quad (5)$$

where ΔASW represents the monthly variation in the available soil water (ASW) stored in the root zone, R_{off} is the monthly surface runoff due to non-infiltrated precipitation, ET_a is the actual crop evapotranspiration computed through the soil water balance, and D_p is deep percolation through the bottom of the root zone.

Other step procedures follow the same Palmer's rules. Negative values of the index indicate a drought episode, and the event ends when the value becomes positive. Table 1 defines the classification of dry and wet events according to the index values. Further information is provided in Pereira et al. [41] and Paulo et al. [42].

2.2.3. Standardized Precipitation Index (SPI) and Reconnaissance Drought Index (RDI)

The SPI was developed by McKee et al. [6] by simply using monthly precipitation data and may be obtained by fitting a probability distribution function to the precipitation accumulated for a desired period, or the time scale. The RDI was proposed by Tsakiris and Vangelis [51] and follows a procedure similar to the SPI, but relative to the ratio between the precipitation and the potential evapotranspiration (P/PET), both aggregated to the time scale. The SPI and the RDI use the same categories of droughts (Table 2).

Table 2. SPI and RDI classifications.

SPI and RDI Values	Category
≥2.00	Extremely wet
1.50 to 1.99	Very wet
1.49 to 1.00	Moderately wet
−0.99 to 0.99	Near normal
−1.00 to −1.50	Moderate drought
−1.50 to −1.99	Severe drought
≤−2.00	Extreme drought

The base information relative to both indices is provided in the previous application to northeast Algeria [5,27]. The calculation of the SPI for any time scale k (9 months in the current application) requires various probability calculation steps [6,52]. The two-parameter gamma distribution was adopted. The cumulative probability derived from the gamma distribution for each precipitation event was then used to obtain the respective standard normal distribution quantile, which is the SPI. A similar approach was used for the RDI relative to the variable P/PET. Positive SPI values refer to a greater-than-median precipitation and dominance of wetness events, while negative values indicate less-than-median precipitation, meaning that a drought is occurring during that selected time period. Events are classified as in Table 2.

Both the SPI and RDI were computed using the DrinC (Drought Indices Calculator) software [53], and the gamma probability distribution function was also used to fit the cumulative records of P and PET in the case of the RDI. The SPI and RDI were computed for the time scale of 9 months, which was more suitable for a comparison with the Sc-PDSI and Med-PDSI, as demonstrated by previous applications in Portugal [41,42,54]. Further details on these indices are provided in the previous studies by Merabti et al. [5,27].

2.3. Drought Spatial and Temporal Analyses

2.3.1. Principal Component Analysis (PCA)

A spatial analysis was conducted, aimed at identifying homogeneous drought regions when computing each of the selected indices. A principal component analysis (PCA) is a multivariate analysis technique that has been applied in several studies as a method of identifying patterns in climatic and hydrological data [55]. This procedure is often used to study drought phenomena [56–60]. The method consists of developing new uncorrelated variables that have linear relationships with the original ones [61]. The purpose is to identify areas that have similar drought patterns in the region. Indeed, an S-mode PCA [62] was applied to the datasets of the four computed indices (Sc-PDSI, MedPDSI, SPI-9, and RDI-9) to be compared. The principal components (PCs) are a sequence of temporal series calculated and arranged in a downward pattern based on their eigenvalues and eigenvectors. The eigenvalues provide information relative to the amount of explained variance by each new variable, while the eigenvectors provide the weight that the original data have in the new components. The PC scores are the normalized values of PCs. The loadings express the observed variable as a function of the PCs and they give a spatial pattern for each PC [58]. A confidence level of 95% was considered to define the number of PCs according to North et al. [63]. The varimax orthogonal rotation was also applied, aimed at obtaining more localized spatial patterns with independent drought variability [5,64].

Experimental semi-variograms were computed using: (i) the RPC1 and RPC2 data, and (ii) the frequency of ED, SD, and MD data in Algeria. A semi-variogram provides the semi-variance between two random variables as the distance between them increases. The nugget variance represents the uncorrelated variation at the scale of sampling, corresponding to the variation that remains unresolved, including any measurement error. The sum of the nugget variance and the spatially correlated variance (partial sill) gives the variance of the random process (total variance or sill). The sill is obtained at a certain range with the pairs of points at their distance or greater, apart and no longer spatially correlated. A linear model with the nugget effect was used for fitting semi-variogram data [65]. Ordinary kriging (OK) was then applied for mapping the spatial interpolation of the patters associated with RCP1 and RCP2, as well as with the frequency of the ED, SD, and MD data, assuming that the data variation is locally stationary when responding to local changes in each indicator. The semi-variogram computation and fitting were carried out with the VESPER software [66] while the implementation of the kriging method was achieved using ArcGIS software (version 10.3; ESRI).

2.3.2. The Modified Mann–Kendall (MMK) Trend Test and Sen's Slope Estimator

The non-parametric modified Mann–Kendall (MMK) trend test [67] was applied to evaluate the statistical significance of the PC score trends retained for the four indices. The original version of the MK test [68,69] was recommended by the World Meteorological Organization [70] to test the monotonic trend of a time series and has been widely used in different fields. However, unlike the MK test, the MMK test takes into account the autocorrelations of a time series; Daufresne et al. [71] reported that the MMK test method was more adequate to test the trends of time series. In the current study, a confidence level of 95% was considered. Thus, the MMK test was used to determine the significance of a trend in a time series combined with Sen's slope estimator [72] to obtain the magnitude of the trend in the PC scores obtained for each sub-region. The detailed calculation method can be found in a previous study [5].

3. Results and Discussion

3.1. Behavior of the Drought Indices

The behavior of the SPI and RDI is already known relative to their previous applications in the same region, both at local and regional levels [5,27]. Numerous applications worldwide are known for the Sc-PDSI, but for the MedPDSI, only information from an application in Portugal is available. Therefore, all indices were applied to all 123 locations and

the results were analyzed. The first application aimed to check if all indices, as expected, would describe the precipitation anomalies, droughts, and wetnesses in a comparable way. Three cases, for a moist sub-humid location in the north and semi-arid and arid sites in the south, are presented in Figure 3 as examples.

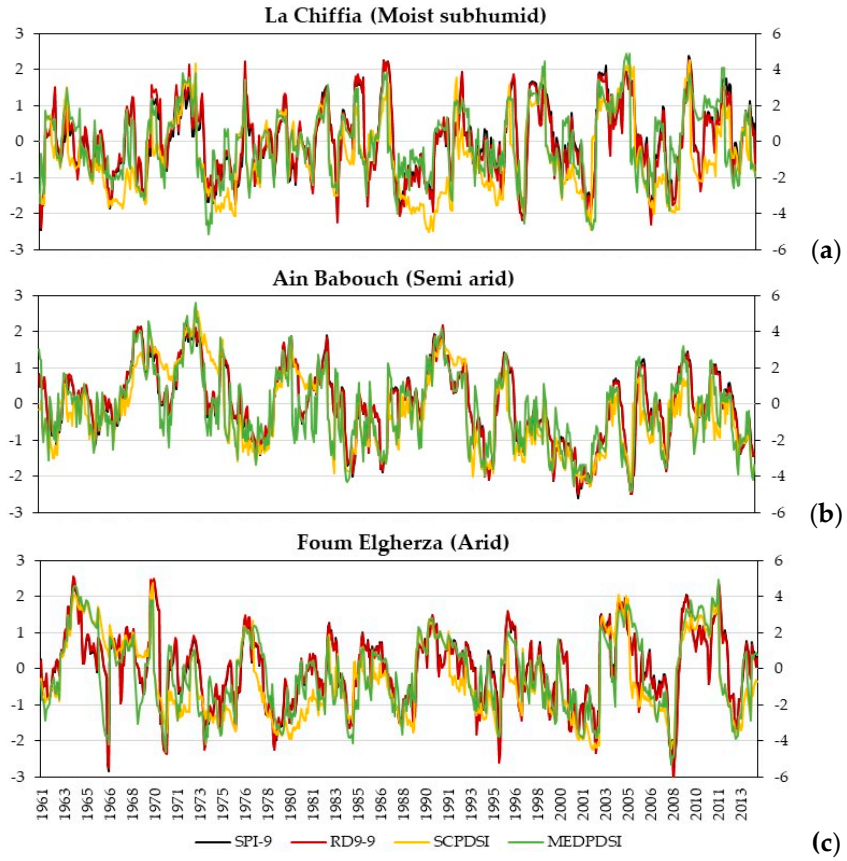

Figure 3. Time series of all drought indices with values for the SPI and RDI on the left OY axis and for the ScPDSI and MedPDSI on the right vertical axis applied to a (**a**) moist sub-humid, (**b**) semi-arid, and (**c**) arid site.

The results of Figure 3 provide evidence that all indices identified the same droughts and wetnesses at each location, but with different severities. To assess this aspect using a general approach, the percent of time in drought in each category was assessed, as represented in Figure 4. The bars in this figure refer to the percent of time in the period of 1961–2014 in extreme (ED), severe (SD), moderate (MD), and mild (mD) droughts, in normal conditions, and in mild (mW), moderate (MW), severe (SW), and extreme (EW) wetnesses.

It can be observed that the indices SPI and RDI behaved very similarly and spent more time in normal conditions (Figure 4). Moreover, they also behaved very similarly for the time spent in any other category of drought, always distinctly from the MedPDSI and, more evidently, from the Sc-PDSI. The latter index identified more drought months than the other three and, of course, showed less time spent as a wetness anomaly. The MedPDSI showed a behavior close to that of the SPI and RDI. All percent values of time in each category agreed with those classically reported by Svoboda et al. [73] for the USA Drought Monitor.

To confirm the partition referred above, a spatial analysis of the percent time spent in the MD, SD, and ED categories was performed, which is represented in Figure 5 using kriging. That spatialization shows again that the SPI and RDI had a similar behavior, particularly with a large area for the same category, MD, and especially SD. These categories are likely the most common, and this result indicates that most of the area was with the same category of drought, either moderate or severe. For the extreme droughts, their

behavior was diverse and revealed that extreme droughts occur more often in sub-humid areas than in semi-arid and arid ones. In fact, these areas are well marked by water scarcity and a few rains are enough to avoid entering into extreme drought, while in the north, the precipitation may decrease to values much lower than the thresholds and, therefore, enter into ED conditions. This spatialization, based upon Lloyd-Hughes and Saunders [74], has not yet been used in the region and, hence, cannot be compared with former studies. The indices based upon the soil water balance behaved differently than those relative to probability thresholds because the MedPDSI progressively adjusts ET_a when the soil water availability decreases. Differently, despite the fact that the Sc-PDSI also has means to decrease the PET demand, it remained high, and the drought condition tended to be higher than for the other indices. Therefore, for the MD and SD categories, the percent of time in drought tended to be higher. This resulted in less time in extreme droughts. The MedPDSI also showed more droughts in the moderate and severe categories, particularly in the semi-arid zone. For the time spent in extreme droughts, the MedPDSI showed a behavior somewhat similar to that of the Sc-PDSI, but with more occurrences.

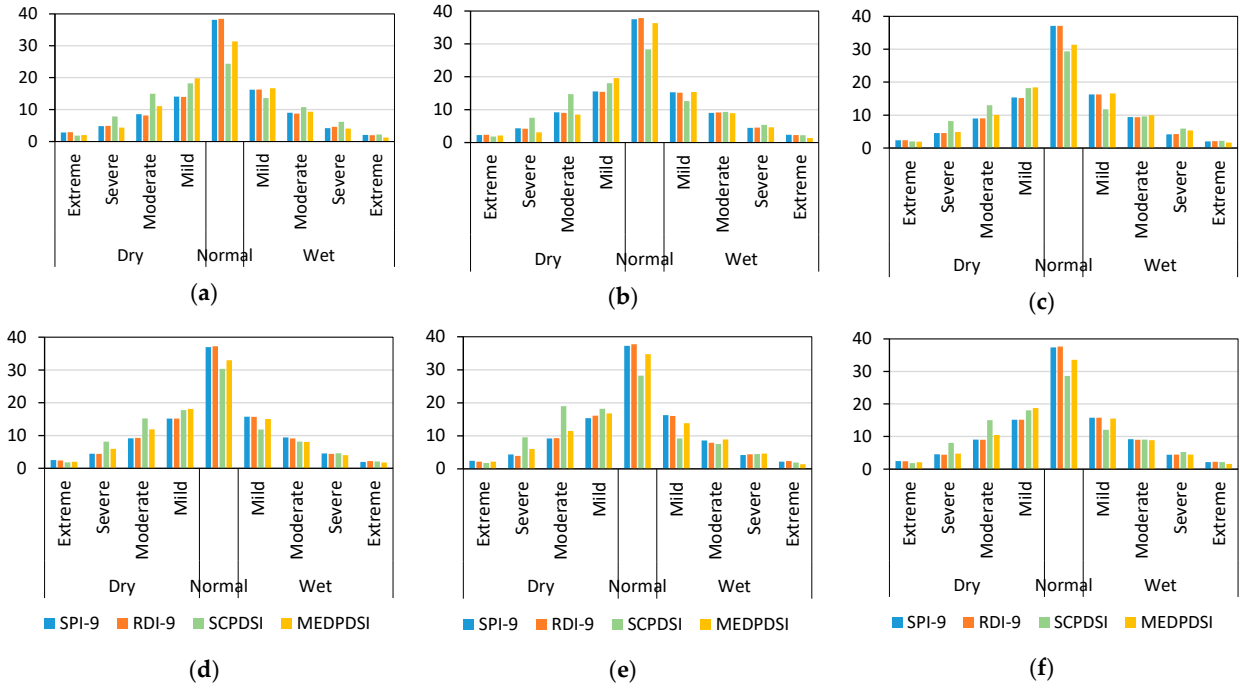

Figure 4. Frequency of drought events when using the different drought indices (SPI-9, RDI-9, Sc-PDSI, and MedPDSI) for the various climate types: (**a**) humid, (**b**) moist sub-humid, (**c**) dry sub-humid, (**d**) semi-arid, (**e**) arid, and (**f**) the full region of northeastern Algeria.

The results in Table 3 show the frequency of EDs; despite the fact that the values of nuggets were lower, the weight of the nuggets in the total variance (i.e., the sum of the nugget with the partial sill) was higher for the MedPDSI and the Sc-PDSI (79.8–83.4%) than for the RDI-9 and the SPI-9 (67–69%). The spatial continuity of the four indices was relatively similar, averaging 31.4 km, which indicates that the occurrence of EDs was local, contrary to SDs and MDs. Yet, because of the nugget effect, the variograms were much different when comparing the MedPDSI and the Sc-PDSI with the RDI-9 and the SPI-9. For the frequency of SDs, the MedPDSI semi-variogram showed a nugget corresponding to only 48.1% of the total variance, while the spatial continuity was the largest (168 km). The parameters of the RDI-9 and SP-I9 semi-variograms were again well aligned, with the nugget value corresponding to 62.0–72.3% of the total variance, and the spatial continuity ranging from 111.5 to 129.0 km, which was thus larger than that for EDs. Differently, the variogram of the Sc-PDSI showed the highest nugget (92.7%) and the lowest range (51.6 km), thus contrasting with all the other indices. Lastly, for the frequency of MDs,

the MEDPDSI semi-variogram again had the lowest nugget value in relation to the total variance (59.4%) and the highest spatial continuity (159 km) when compared with all other indices. In all three of the other indices, and like for ED and SD, the variation occurring at smaller scales than that modelled by the variograms was quite large, representing 72.6 to 89.6% of the total variance. The Sc-PDSI presented with the largest RMSE and AIC values, showing some possible inadequacy of the computed variogram or possible limitations of the self-calibration method, as noted by Dai et al. [75].

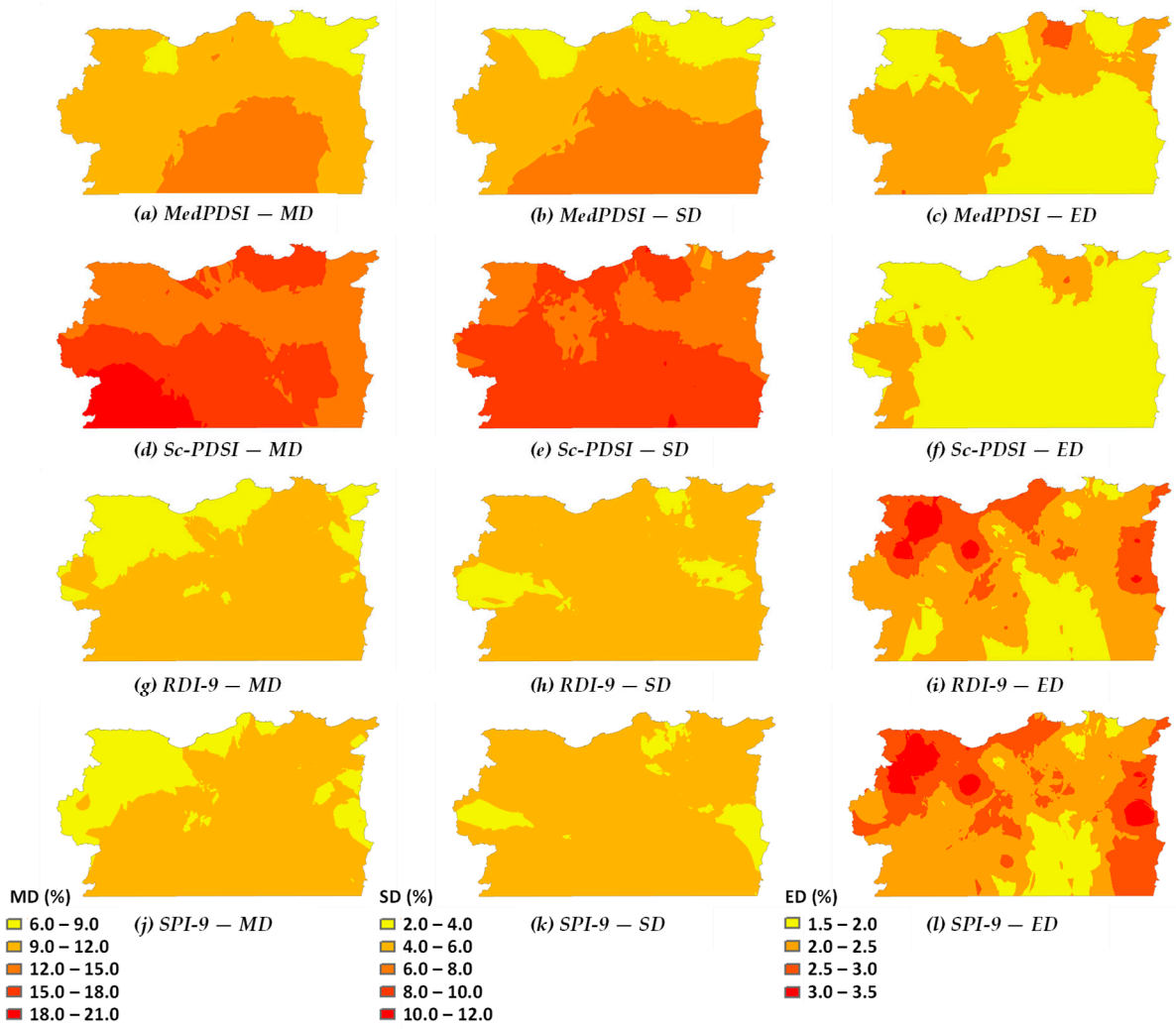

Figure 5. Spatial distribution of percent of time spent in the moderate, severe, and extreme categories of drought (MD, SD, ED) at each location in northeastern Algeria when using the four different indices MedPDSI (**a**–**c**), Sc-PDSI (**d**–**f**), RDI (**g**–**i**) and SPI (**j**–**l**).

Table 3. Details of the parameters of the covariance linear models fitted to the distribution of time spent in the moderate, severe, and extreme categories of drought at each location.

Variable	Nugget	Partial Sill	Range (m)	RMSE	AIC
MedPDSI ED	0.2578	0.0653	33,107	0.0238	−49.90
Sc-PDSI ED	0.2442	0.0486	23,517	0.0236	−50.06
RI-9 ED	0.5592	0.2507	35,978	0.1008	−18.11
SPI-9 ED	0.5732	0.2829	33,068	0.1027	−17.70
MedPDSI SD	2.2440	2.4260	168,022	0.1549	−8.65
Sc-PDSI SD	9.7900	0.7759	51,592	0.3689	10.44

Table 3. *Cont.*

Variable	Nugget	Partial Sill	Range (m)	RMSE	AIC
RI-9 SD	0.8527	0.3267	111,550	0.0535	−32.02
SPI-9 SD	0.8667	0.5316	128,980	0.1991	−3.13
MedPDSI MD	4.0610	2.7810	158,959	0.3996	12.20
Sc-PDSI MD	7.7280	2.9190	73,205	1.3070	38.27
RID-9 MD	2.2920	0.4493	30,052	0.1580	−8.21
SPI-9 MD	2.3430	0.2711	27,289	0.1206	−14.15

Notes: ED—extreme drought; SD—severe drought; MD—moderate drought; RMSE—root mean square error; AIC—Akaike information criteria.

3.2. Spatial Patterns of Droughts

The application of a principal component analysis to the four indices referred to before led to the retention of two principal components (PCs), which were then rotated using the varimax rotation by following North's rule [63] and conducting a thorough screening of the scree plots of the eigenvalues of the PCs analyzed, hence assuming that the other components were less important and might not be considered. Each PC identified a sub-region characterized by a different drought variability and precipitation regime. Table 4 shows the explained variances of the varimax-rotated PCs relative to each index, while Figure 6 indicates the spatial patterns of the PCs.

Table 4. Explained variance (%) of the principal components after varimax rotation.

	Explained Variance (%)		
	PC1	**PC2**	**Cumulative**
Sc-PDSI	33.8	27.3	61.1
MedPDSI	33.2	24.7	57.9
SPI-9	42.1	27.7	69.8
RDI-9	42.4	29.2	71.5

The first PC explained more than 33% of the total variance for both the MedPDSI and Sc-PDSI series, while for the SPI-9 and RDI-9, PC1 reached 42% of the total variance. The contribution rate of the cumulative variability of the two principal components retained was 61.1% and 57.9% for the Sc-PDSI and the MedPDSI, respectively, and this value was greater for the SPI and RDI, which exceeded 69.8% and 71.5%, respectively. These values for the SPI and RDI were very similar due to the also similar probabilistic nature of both indices. The Sc-PDSI and MedPDSI had lower percentages of explanation for their variability, but both indices behaved similarly. To illustrate the spatial patterns of drought variability, the rotated loadings corresponding to both PC1 and PC2 were mapped (Figure 6) for all indices. The results showed two distinct sub-regions. The first component refers to the northern sub-region for the four indices, but with differences in the total areas identified. The patterns of the RDI-9 and SPI-9 were very similar, which reflects the fact their values relative to PC1 were very close, at 42.1% and 42.4%, respectively. Differently, the spatial patterns of the MedPDSI and Sc-PDSI, particularly the MedPDSI, identified a small area in the northeastern part that was characterized by a higher precipitation regime. PC2 refers to the southern sub-region, which is known for its aridity, low precipitation, and high temperature, PET, and ET_o. Even though there was no great difference between the loading values of the indices in the southern sub-region, the identified areas were greater for the SPI-9 and RDI-9 than those detected by the MedPDSI and Sc-PDSI, especially by the Sc-PDSI. The effects of PET in the RDI were not detected in both PC loadings, since the RDI values were identical to the SPI ones. Differently, the results for the MedPDSI and Sc-PDSI that used, respectively, olive crop evapotranspiration and reference evapotranspiration to perform the water balance showed that these indices behaved differently from the former indices. The results agree with former studies by Merabti et al. [5] and Taibi et al. [76].

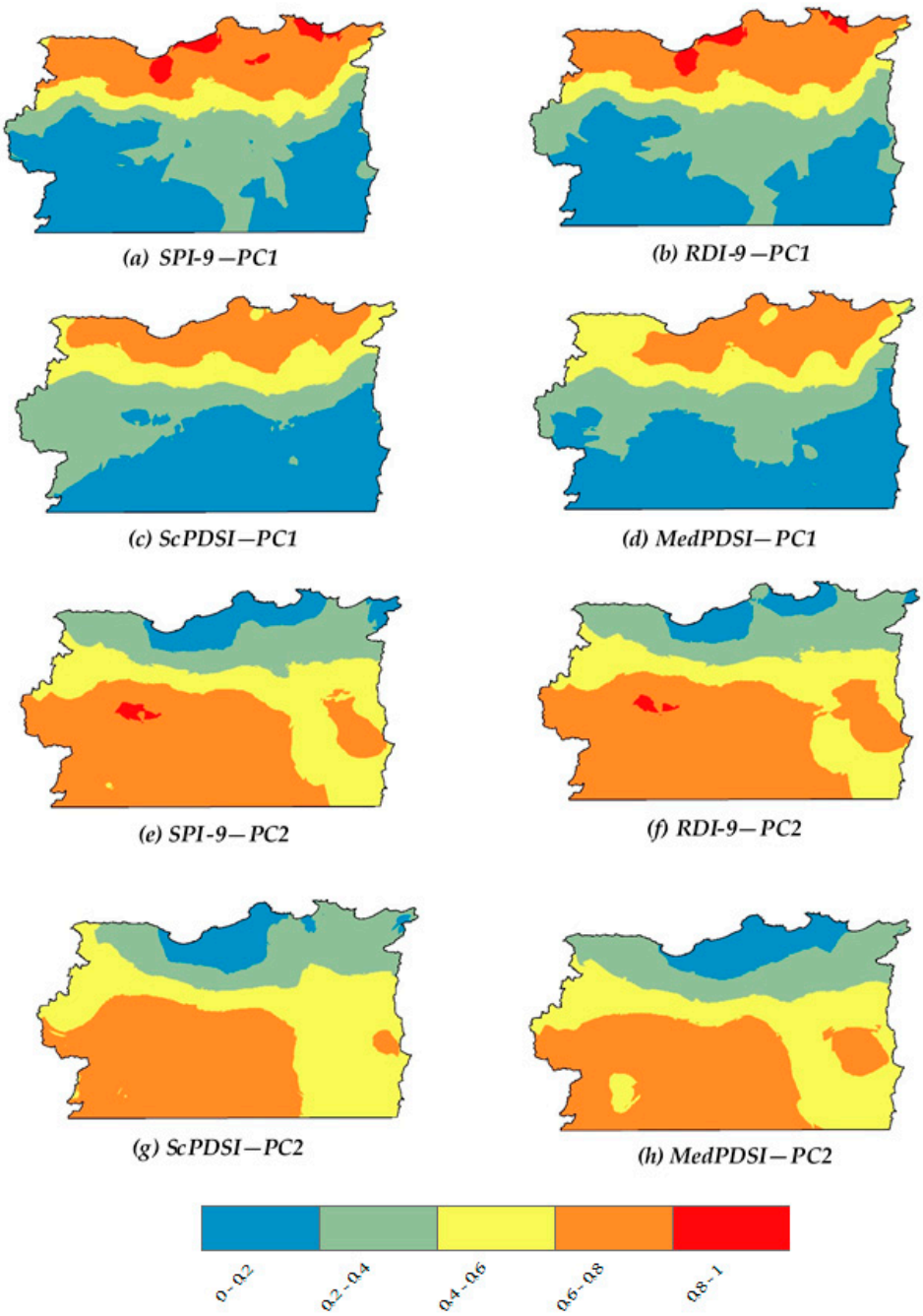

Figure 6. Varimax-rotated loadings relative to PC1 (**a**–**d**) and PC2 (**e**–**h**) using SPI-9, RDI-9, Sc-PDSI, and MedPDSI.

For RPC1 and RPC2, the nugget values, obtained when fitting the linear model, corresponded, respectively and on average, to 25.6 and 40.8% of the total variance (i.e., sum of the nugget with partial sill) (Table 5). The lowest value was found for the MedPDSI RPC1 (14.0%), while the highest was found for the Sc-PDSI RPC2 (54.6%). These values were explained by the distribution of the meteorological stations used, and the variation that occurs at scales too small to properly characterize that distribution. The spatial continuity ranged from 50.7 to 82.7 km for RPC1 and from 50.0 to 69.3 km for RPC2; thus, they were relatively similar. The spatial continuity was highest for the MedPDSI in both RPC1 and RPC2. The results above may indicate that the MedPDSI consists of a drought index that is very appropriate for the Mediterranean region.

Table 5. Parameters of the data covariance linear model fitted to the varimax-rotated loadings relative to the MedPDSI, ScPDSI, RDI-9, and SPI-9.

Variable	Nugget	Partial Sill	Range (m)	RMSE	AIC
MedPDSI RPC1	0.0041	0.0252	82,727	0.038	−90.07
MedPDSI RPC2	0.0078	0.0131	69,312	0.033	−98.48
Sc-PDSI RPC1	0.0122	0.0134	55,152	0.049	−74.43
Sc-PDSI RPC2	0.0194	0.0161	55,152	0.032	−100.70
RDI-9 RPC1	0.0047	0.0148	50,680	0.066	−56.33
RDI-9 RPC2	0.0066	0.0109	50,000	0.040	−86.68
SPI-9 RPC1	0.0036	0.0180	55,152	0.069	−56.46
SPI-9 RPC2	0.0063	0.0126	50,680	0.041	−85.70

Notes: RPC—rotated principal component; RMSE—root mean square error; AIC—Akaike information criteria.

3.3. Trend Analysis of Droughts

Across the 54-year study period, the overall inter-comparison of the trend analysis between the four drought indices was complex. Indeed, by using the MMK test, a trend analysis was performed on the rotated PC scores associated with each drought index. Twelve time series sets relative to each month's values and one relative to the yearly values of each index were extracted, and the significance levels of the MMK test and Sen's slope trends are presented in Table 6.

The climatology of both detected sub-regions is likely different, and their behavior is distinct relative to the droughts noted between the two sub-regions (Table 6). Indeed, all the drought indices showed significant trends toward a decrease in the frequency and severity of droughts for a few months in the northern sub-region, and for the full year in the case of the Sc-PDSI; differently, in the southern sub-region, the MMK and Sen's slope indicated significant trend toward an increase in the frequency and severity of droughts in several months, more so in the case of the Sc-PDSI and the MedPDSI. Hence, the frequency and severity of droughts tended to decrease in the north and increase in the south.

The RDI monthly test values for PC1 and PC2 showed the same trends as the other indices, but they were significant only for the year in the case of RPC1, and in June and July for RPC2, i.e., there was no evidence of significant impacts of climate change. The SPI-9 showed similar results for the MMK and Sen's tests, but these were significant for seven months; however, the winter was excluded in the case of PC1 and only four months were significant in the case of PC2, mostly occurring in the spring season. Therefore, both probabilistic indices did not significantly identify the influence of climate change on the drought regime.

These results agree with those of a former study in the same region [27] that used a different approach for estimating PET. Differently, both indices based on the soil water balance indicated climate change influences, with nine months and the year showing significant trends relative to PC1 using the MedPDSI, or seven monthly series for PC2; in the case of the Sc-PDSI, all months showed a significant positive trend for the northern region, but just four months with a significant negative trend for the southern sub-region, mainly occurring in the spring. The results indicated that the arid and semi-arid regions tended to be more exposed and vulnerable to droughts.

The time series of RPC1 and RPC2 relative to the four indices clearly showed trends throughout 1961–2014 (Figure 7). The slopes were positive for RPC1 and quite similar for the four indices, thus confirming the trends detected for all months by the MMK and Sen's tests, independently of their significancy. Similarly, there was also an overall confirmation of the negative trends for the southern sub-region, but with a larger slope in the case of the Sc-PDSI and MedPDSI, as shown by the analysis in Table 6.

Table 6. Trend analysis of the rotated PC scores relative to all four indices, using the modified Mann-Kendal test, and magnitude of trends using Sen's slope for the period of 1961 to 2014.

	RDI-9				SPI-9			
	RPC1		RPC2		RPC1		RPC2	
	MMK	Sen's Slope	MMK	Sen's Slope	MMK	Sen's Slope	MMK	Sen's Slope
Jan	0.084	0.013	0.338	−0.012	0.131	0.014	0.369	−0.008
Feb	0.195	0.009	0.131	−0.013	0.300	0.010	0.812	−0.002
Mar	0.082	0.014	0.211	−0.014	0.052	0.017	0.607	−0.006
Apr	0.087	0.014	0.206	−0.014	0.042	0.018	0.466	−0.008
May	0.099	0.015	0.109	−0.017	0.026	0.016	0.505	−0.007
Jun	0.217	0.012	0.045	−0.021	0.102	0.013	0.247	−0.010
Jul	0.093	0.012	0.034	−0.022	0.036	0.017	0.361	−0.011
Aug	0.476	0.006	0.071	−0.019	0.020	0.018	0.338	−0.010
Sep	0.332	0.009	0.216	−0.011	0.016	0.021	0.355	−0.010
Oct	0.551	0.005	0.571	−0.005	0.019	0.021	0.132	−0.016
Nov	0.170	0.012	0.379	−0.008	0.016	0.019	0.069	−0.019
Dec	0.161	0.012	0.289	−0.010	0.179	0.012	0.136	−0.017
Year	0.041	0.014	0.098	−0.013	0.008	0.017	0.251	−0.009
	MedPDSI				ScPDSI			
	RPC1		RPC2		RPC1		RPC2	
	MMK	Sen's Slope	MMK	Sen's Slope	MMK	Sen's Slope	MMK	Sen's Slope
Jan	0.003	0.029	0.102	−0.013	0.009	0.023	0.216	−0.011
Feb	0.014	0.026	0.012	−0.023	0.023	0.023	0.095	−0.017
Mar	0.001	0.030	0.018	−0.024	0.007	0.026	0.032	−0.019
Apr	0.017	0.023	0.041	−0.022	0.020	0.023	0.032	−0.018
May	0.008	0.025	0.022	−0.023	0.011	0.020	0.052	−0.018
Jun	0.026	0.018	0.031	−0.026	0.032	0.021	0.046	−0.019
Jul	0.033	0.018	0.033	−0.021	0.029	0.021	0.049	−0.017
Aug	0.066	0.018	0.062	−0.016	0.038	0.020	0.095	−0.015
Sep	0.101	0.014	0.310	−0.011	0.034	0.019	0.179	−0.012
Oct	0.110	0.014	0.289	−0.010	0.037	0.021	0.148	−0.012
Nov	0.026	0.022	0.047	−0.016	0.009	0.025	0.086	−0.014
Dec	0.015	0.024	0.052	−0.018	0.006	0.023	0.098	−0.015
Year	0.009	0.021	0.015	−0.020	0.008	0.021	0.069	−0.015

The differences among the drought indices may be tentatively explained. The RDI-9 combines the probabilities relative to the variables of precipitation (P) and PET, while the SPI-9 just uses the monthly precipitation with P described by the gamma distribution function. Differently, the MedPDSI and Sc-PDSI define the index after performing the soil water balance of a perennial olive orchard (for the former) and by using ET_o (in the latter), thus allowing the index to indicate when insufficient natural water availability creates water stress or, otherwise, surplus. This helps to explain the reason for the negative drought trend in the southern, more arid, sub-region, since water stress occurs more easily and more often there. Such trends of drought increasing in the southern sub-region and decreasing in the northern area were observed in a previous study by Merabti et al. [27] using only the SPI and RDI, and by Bessaklia et al. [77] relative to the precipitation in the study region.

Mrad et al. [78] also reported in the same direction after studying the time evolution of precipitation in the Constantine plateau, which is in the transition zone of the current study area. A tentative explanation for this difference in drought trends has been proposed by Taibi et al. [26]. Zerouali et al. [79] used a very different approach by studying the regionalization of rainfall patterns based on wavelet transform information and a hierarchical cluster analysis in northeastern Algeria. They found three clusters, with the first and part of the second within the identified northern sub-region and cluster 3 and part of cluster 2

within the southern sub-region. However, they focused on periodic annual precipitation fluctuations that do not yet help explain the drought trends identified in the current study.

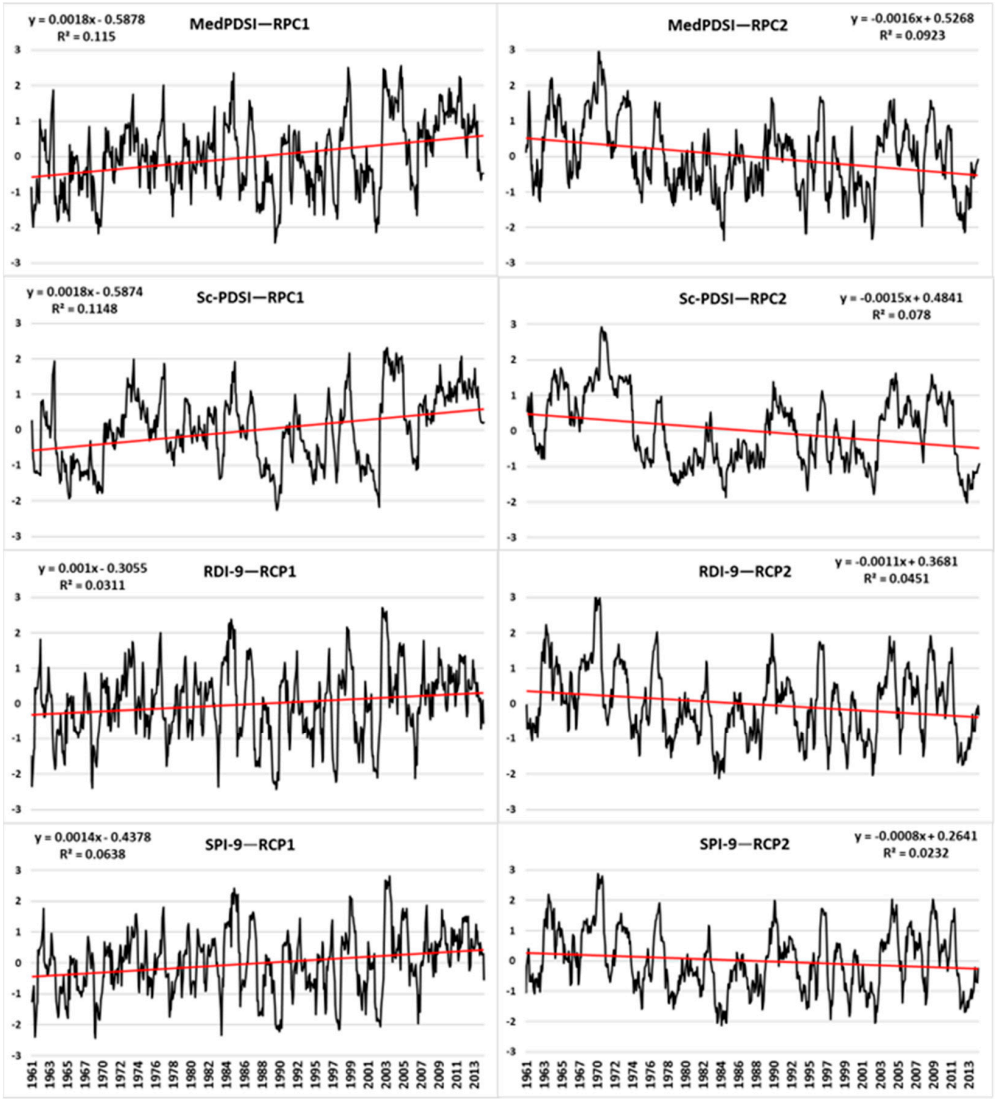

Figure 7. Time variability of the rotated PC1 and PC2 scores relative to MedPDSI, Sc-PDSI, RDI-9, and SPI-9 for northeastern Algeria, 1961–2014.

The occurrence of contradictory trends inside a region has been reported by various authors, e.g., Di Lena et al. [80]. However, a study focusing on the Mediterranean region [81] just reported on an increase in drought frequency and severity. Hence, the causes for these contradictory trends remain an open question that requires a better understanding of the combined effects of the atmospheric circulation and of the Atlas chain, which starts developing near the north coast. The current knowledge of trends is nevertheless very important for supporting water and agricultural policies and for establishing warning systems, mainly focused on agriculture.

4. Conclusions

This research focused on the spatiotemporal evolution of droughts in northeastern Algeria over the period of 1961–2014 and the spatial distribution of the percentual duration of the moderate, severe, and extreme categories of drought. The drought indices used were the PDSI, MedPDSI, RDI-9, and SPI-9.

A first conclusion is that all drought indices behaved concordantly, with both probabilistic indices, the SPI and RDI, producing very close results, but with different results produced by both the soil water balance indices. The novel PDSI (MedPDSI) behaved concordantly to the SPI and RDI but distinctly from the Sc-PDSI. It showed less time in the normal condition than the latter and more time in the normal condition than the former ones. The distribution of time in the various drought and wetness categories were all in agreement with that occurring in the Drought Monitor used in the USA with various drought indices. An innovative approach consisted of the spatialization of the time in each MD, SD, and ED category, which showed a different behavior in the drought indices, with the MedPDSI close to the SPI-9 and RDI-9 for moderate and severe droughts, but closer to the Sc-PDSI for extreme droughts. The variogram results also confirmed the good behavior of the MedPDSI and questioned that of the Sc-PDSI, as referred to in Section 3.1. This approach requires further study in other Mediterranean areas.

The results call attention to the quality of weather data used to compute drought indices and, particularly, to compute evapotranspiration. Very numerous studies have been published in the last decade about equations that could replace the FAO56 PM-ET_o when data are missing, but few studies have focused on the effect of the quality of data used, in particular, the data used for computing drought indices. The results in this study demonstrate that using different approaches to compute the soil water balance (using potential vs. actual ET) leads to a different behavior of the PDSI indices, apparently in favor of the ET_a used in the MedPDSI. Assuming that this is true, developing an appropriate software is essential, which could also include support for data quality testing.

The application of PCA in S-mode with varimax rotation to the four indices led to the obtaining of the spatial patterns of drought and wetness events in northeastern Algeria. The results for all indices identified two sub-regions with different spatial patterns of drought variability and different temporal behavior. The first PC represented and concentrated majorly in the northern sub-region, which mostly corresponds to humid and sub-humid climates, with the four indices showing differences regarding the scores and the total areas identified. The MedPDSI was more reactive to the Mediterranean rainfall regime, and the SPI and RDI were very much similar between them. The second component corresponded to the southern sub-region, with semi-arid and arid climates. The spatial patterns of droughts are caused by the distance to the Mediterranean Sea and by the Atlas Mountain range, which increases in elevation to the south and consists of a barrier to the rainfall that progressively decreases with the elevation in the south of that large mountain range.

Trends were detected with the MMK test and Sen's slope test applied to both the RPC scores associated with every drought index. Despite the fact that non-significant results were the most frequent, the tests evidenced trends of a decrease in drought occurrence and severity in the northern sub-region and an increase in the southern sub-region. This contradictory condition was identified just for northeastern Algeria, since generally increasing trends have been reported for the Mediterranean basin. This condition calls for research focusing on the atmosphere circulation patterns combined with the effects of the Atlas Mountain range.

Author Contributions: Conceptualization and methodology, L.S.P. and A.M.; data curation, A.M. and M.M.; formal analysis, A.M., H.D. and P.P.; writing—original draft preparation, A.M. and H.D.; writing—review and editing, A.M., P.P., M.M. and L.S.P.; visualization, H.D. All authors have read and agreed to the published version of the manuscript.

Funding: This research received no external funding but the operational support of the Fundação para a Ciência e a Tecnologia, Portugal, through the grant attributed to the research unit LEAF—Linking Landscape, Environment, Agriculture and Food—Research Centre (UIDB/04129/2020 and UIDP/04129/2020) and the research fellowships to H. Darouich (CEECIND/01153/2017) and P. Paredes (DL 57/2016/CP1382/CT0022), which are acknowledged.

Data Availability Statement: Not applicable.

Acknowledgments: The authors thank the National Hydraulic Resources Agency for the availability of precipitation data and the Climate Research Unit Time Series (CRU-TS v. 4.06), University of East Anglia, United Kingdom, for access to potential evapotranspiration data.

Conflicts of Interest: The authors declare no conflict of interest.

References

1. Pereira, L.S.; Cordery, I.; Iacovides, I. *Coping with Water Scarcity: Addressing the Challenges*; Springer: Dordrecht, The Netherlands, 2009.
2. Pires, C.A.L.; Pereira, L.S. (Eds.) *Predictabilidade Sazonal de Secas—Avaliação ao Nível Regional e Agrícola*; ISA Press: Lisbon, Portugal, 2015; (In Portuguese). [CrossRef]
3. Tsakiris, G. Drought risk assessment and management. *Water Resour. Manag.* **2017**, *31*, 3083–3095. [CrossRef]
4. Tramblay, Y.; Koutroulis, A.; Samaniego, L.; Vicente-Serrano, S.M.; Volaire, F.; Boone, A.; Le Page, M.; Llasat, M.C.; Albergel, C.; Burak, S.; et al. Challenges for Drought Assessment in the Mediterranean region under future climate scenarios. *Earth-Sci Rev* **2020**, *210*, 103348. [CrossRef]
5. Merabti, A.; Martins, D.S.; Meddi, M.; Pereira, L.S. Spatial and time variability of drought based on SPI and RDI with various time scales. *Water Resour. Manag.* **2018**, *32*, 1087–1100. [CrossRef]
6. McKee, T.B.; Doesken, N.J.; Kleist, J. The relationship of drought frequency and duration to time scales. In Proceedings of the 8th Conference on Applied Climatology, Boston, MA, USA, 17–22 January 1993; pp. 179–184.
7. Tsakiris, G.; Pangalou, D.; Vangelis, H. Regional drought assessment based on the reconnaissance drought index (RDI). *Water Resour. Manag.* **2007**, *21*, 821–833. [CrossRef]
8. Ripple, W.J.; Wolf, C.; Gregg, J.W.; Levin, K.; Rockström, J.; Newsome, T.M.; Betts, M.G.; Huq, S.; Law, B.E.; Kemp, L.; et al. World scientists' warning of a climate emergency 2022. *BioScience* **2022**, *72*, 1149–1155. [CrossRef]
9. Hoerling, M.; Eischeid, J.; Perlwitz, J.; Quan, X.; Zhang, T.; Pegion, P. On the increased frequency of Mediterranean drought. *J. Clim.* **2012**, *25*, 2146–2161. [CrossRef]
10. Giorgi, F.; Lionello, P. Climate change projections for the Mediterranean region. *Glob. Planet. Change* **2008**, *63*, 90–104. [CrossRef]
11. Sousa, P.M.; Trigo, R.M.; Aizpurua, P.; Nieto, R.; Gimeno, L.; Garcia-Herrera, R. Trends and extremes of drought indices throughout the 20th century in the Mediterranean. *Nat. Hazards Earth Syst. Sci.* **2011**, *11*, 33–51. [CrossRef]
12. Moreira, E.; Pires, C.; Pereira, L. SPI Drought Class Predictions driven by the North Atlantic Oscillation index using log-linear modeling. *Water* **2016**, *8*, 43. [CrossRef]
13. Hallouz, F.; Meddi, M.; Mahé, G.; Ali Rahmani, S.; Karahacane, H.; Brahimi, S. Analysis of meteorological drought sequences at various timescales in semi-arid climate: Case of the Cheliff watershed (Northwest of Algeria). *Arab. J. Geosci.* **2020**, *13*, 280. [CrossRef]
14. Spinoni, J.; Naumann, G.; Carrao, H.; Barbosa, P.; Vogt, J. World drought frequency, duration, and severity for 1951–2010. *Int. J. Climatol.* **2014**, *34*, 2792–2804. [CrossRef]
15. Stagge, J.H.; Kingston, D.G.; Tallaksen, L.M.; Hannah, D.M. Observed drought indices show increasing divergence across Europe. *Sci. Rep.* **2017**, *7*, 14045. [CrossRef] [PubMed]
16. Moreira, E.E.; Mexia, J.T.; Pereira, L.S. Are drought occurrence and severity aggravating? A study on SPI drought class transitions using log-linear Models and ANOVA-like inference. *Hydrol. Earth Syst. Sci.* **2012**, *16*, 3011–3028. [CrossRef]
17. Domínguez-Castro, F.; Vicente-Serrano, S.M.; Tomás-Burguera, M.; Peña-Gallardo, M.; Beguería, S.; Kenawy, A.; Luna, Y.; Morata, A. High spatial resolution climatology of drought events for Spain: 1961–2014. *Int. J. Climatol.* **2019**, *39*, 5046–5062. [CrossRef]
18. Vicente-Serrano, S.M.; Domínguez-Castro, F.; Murphy, C.; Hannaford, J.; Reig, F.; Peña-Angulo, D.; Tramblay, Y.; Trigo, R.M.; Mac Donald, N.; Luna, M.Y.; et al. Long-term variability and trends in meteorological droughts in western Europe (1851–2018). *Int. J. Climatol.* **2021**, *41* (Suppl. 1), E690–E717. [CrossRef]
19. Lloyd-Hughes, B. The Impracticality of a universal drought definition. *Theor. Appl. Climatol.* **2014**, *117*, 607–611. [CrossRef]
20. Wilhite, D.A.; Pulwarty, R.S. Drought as hazard: Understanding the natural and social context. In *Drought and Water Crises: Integrating Science, Management, and Policy*, 2nd ed.; Wilhite, D., Pulwarty, R.S., Eds.; CRC Press: Boca Raton, FL, USA, 2017; pp. 3–20. [CrossRef]
21. Tanasijevic, L.; Todorovic, M.; Pereira, L.S.; Pizzigalli, C.; Lionello, P. Impacts of climate change on olive crop evapotranspiration and irrigation requirements in the Mediterranean region. *Agric. Water Manag.* **2014**, *144*, 54–68. [CrossRef]
22. Saadi, S.; Todorovic, M.; Tanasijevic, L.; Pereira, L.S.; Pizzigalli, C.; Lionello, P. Climate change and Mediterranean agriculture: Impacts on winter wheat and tomato crop evapotranspiration, irrigation requirements and yield. *Agric. Water Manag.* **2015**, *147*, 103–115. [CrossRef]
23. Pulwarty, S.R.; Sivakumar, M.V.K. Information systems in a changing climate: Early warnings and drought risk management. *Weather. Clim. Extrem.* **2014**, *3*, 14–21. [CrossRef]
24. Meddi, M.M.; Assani, A.A.; Meddi, H. Temporal variability of annual rainfall in the Macta and Tafna catchments, northwestern Algeria. *Water Resour. Manag.* **2010**, *24*, 3817–3833. [CrossRef]
25. Hamlaoui-Moulai, L.; Mesbah, M.; Souag-Gamane, D.; Medjerab, A. Detecting hydro-climatic change using spatiotemporal analysis of rainfall time series in western Algeria. *Nat. Hazards* **2013**, *65*, 1293–1311. [CrossRef]

26. Taibi, S.; Meddi, M.; Mahé, G.; Assani, A. Relationships between atmospheric circulation indices and rainfall in northern Algeria and comparison of observed and RCM-generated rainfall. *Theor. Appl. Climatol.* **2017**, *127*, 241–257. [CrossRef]
27. Merabti, A.; Meddi, M.; Martins, D.S.; Pereira, L.S. Comparing SPI and RDI applied at local scale as influenced by climate. *Water Resour. Manag.* **2018**, *32*, 1071–1085. [CrossRef]
28. Meddi, M.; Meddi, H.; Toumi, S.; Mehaigue, M. Regionalization of rainfall in north-western Algeria. *Geogr. Tech.* **2013**, *17*, 56–69.
29. Habibi, B.; Meddi, M.; Torfs, P.J.J.F.; Remaoun, M.; Van Lanen, H.A.J. Characterisation and prediction of meteorological drought using stochastic models in the semi-arid Chéliff–Zahrez basin (Algeria). *J. Hydrol. Reg. Stud.* **2018**, *16*, 15–31. [CrossRef]
30. Habibi, B.; Meddi, M. Meteorological drought hazard analysis of wheat production in the semi-arid basin of Cheliff–Zahrez nord, Algeria. *Arab. J. Geosci.* **2021**, *14*, 1045. [CrossRef]
31. Vicente-Serrano, S.M.; Beguería, S.; López-Moreno, J.I. A Multiscalar drought index sensitive to global warming: The standardized precipitation evapotranspiration index. *J. Clim.* **2010**, *23*, 1696–1718. [CrossRef]
32. Palmer, W. *Meteorological Drought*; U.S. Weather Bureau: Washington, DC, USA, 1965.
33. Thornthwaite, C.W. An approach toward a rational classification of climate. *Geogr. Rev.* **1948**, *38*, 55–94. [CrossRef]
34. Werick, W.J.; Willeke, G.E.; Guttman, N.B.; Hosking, J.R.M.; Wallis, J.R. National drought atlas developed. *EOS* **1994**, *75*, 89–90. [CrossRef]
35. Nalbantis, I.; Tsakiris, G. Assessment of hydrological drought revisited. *Water Resour. Manag.* **2009**, *23*, 881–897. [CrossRef]
36. Wu, H.; Hayes, M.J.; Weiss, A.; Hu, Q. An evaluation of the standardized precipitation index, the China-Z index and the statistical Z-score. *Int. J. Clim.* **2001**, *21*, 745–758. [CrossRef]
37. Morid, S.; Smakhtin, V.; Moghaddasi, M. Comparison of seven meteorological indices for drought monitoring in Iran. *Int. J. Clim.* **2006**, *26*, 971–985. [CrossRef]
38. Byun, H.R.; Wilhite, D.R. Objective quantification of drought severity and duration. *J. Clim.* **1999**, *12*, 2747–2756. [CrossRef]
39. Ogunrinde, A.T.; Oguntunde, P.G.; Olasehinde, D.A.; Fasinmirin, J.T.; Akinwumiju, A.S. Drought spatiotemporal characterization using self-calibrating Palmer drought severity index in the northern region of Nigeria. *Results Eng.* **2020**, *5*, 100088. [CrossRef]
40. Wells, N.; Goddard, S.; Hayes, M.J. A self-calibrating Palmer drought severity index. *J. Clim.* **2004**, *17*, 2335–2351. [CrossRef]
41. Pereira, L.S.; Rosa, R.D.; Paulo, A.A. Testing a modification of the Palmer drought severity index for Mediterranean environments. In *Methods and Tools for Drought Analysis and Management*; Rossi, G., Vega, T., Bonaccorso, B., Eds.; Springer: Dordrecht, The Netherlands, 2007; Volume 62, pp. 149–167. [CrossRef]
42. Paulo, A.; Martins, D.S.; Paredes, P.; Rosa, R.D.; Pereira, L.S. Modification of the Palmer drought severity index for Mediterranean environments. *Eur. Water* **2017**, *60*, 195–201.
43. Karl, T.R.; Williams, C.N. An approach to adjusting climatological time series for discontinuous inhomogeneities. *J. Appl. Meteorol. Climatol.* **1987**, *26*, 1744–1763. [CrossRef]
44. Allen, R.G.; Pereira, L.S.; Raes, D.; Smith, M. *Crop Evapotranspiration-Guidelines for Computing Crop Water Requirements*; FAO Irrigation and Drainage Paper 56; FAO: Rome, Italy, 1998; p. 300.
45. Harris, I.; Osborn, T.J.; Jones, P.; Lister, D. Version 4 of the CRU TS monthly high-resolution gridded multivariate climate dataset. *Sci. Data* **2020**, *7*, 109. [CrossRef]
46. Harris, I.; Jones, P.D.; Osborn, T.J.; Lister, D.H. Updated high-resolution grids of monthly climatic observations—The CRU TS3.10. *Int. J. Climatol.* **2014**, *34*, 623–642. [CrossRef]
47. Ahmed, K.; Shahid, S.; Sachindra, D.A.; Nawaz, N.; Chung, E.-S. Fidelity assessment of general circulation model simulated precipitation and temperature over Pakistan using a feature selection method. *J. Hydrol.* **2019**, *573*, 281–298. [CrossRef]
48. Oduro, C.; Shuoben, B.; Ayugi, B.; Beibei, L.; Babaousmail, H.; Sarfo, I.; Ullah, S.; Ngoma, H. Observed and coupled model intercomparison Project 6 multimodel simulated changes in near-surface temperature properties over Ghana during the 20th century. *Int. J. Climatol.* **2022**, *42*, 3681–3701. [CrossRef]
49. Pour, S.H.; Wahab, A.K.A.; Shahid, S. Spatiotemporal changes in aridity and the shift of drylands in Iran. *Atmospheric Res.* **2020**, *233*, 104704. [CrossRef]
50. Rosa, R.D.; Paredes, P.; Rodrigues, G.C.; Alves, I.; Fernando, R.M.; Pereira, L.S.; Allen, R.G. Implementing the dual crop coefficient approach in interactive software. 1. Background and computational strategy. *Agr. Water Manag.* **2012**, *103*, 8–24. [CrossRef]
51. Tsakiris, G.; Vangelis, H.J.E.W. Establishing a drought index incorporating evapotranspiration. *Eur. Water* **2005**, *9*, 3–11.
52. Guttman, N.B. Accepting the standardized precipitation index: A calculation algorithm. *J. Am. Water Resour. Assoc.* **1999**, *35*, 311–322. [CrossRef]
53. Tigkas, D.; Vangelis, H.; Tsakiris, G. DrinC: A software for drought analysis based on drought indices. *Earth Sci. Inform.* **2015**, *8*, 697–709. [CrossRef]
54. Paulo, A.A.; Rosa, R.D.; Pereira, L.S. Climate trends and behaviour of drought indices based on precipitation and evapotranspiration in Portugal. *Nat. Hazards Earth Syst. Sci.* **2012**, *12*, 1481–1491. [CrossRef]
55. Smith, L.I. *A tutorial on principal components analysis. Computer Sciences*, 26th ed.; University of Otago: Dunedin, New Zealand, 2002.
56. Prajapati, V.K.; Khanna, M.; Singh, M.; Kaur, R.; Sahoo, R.N.; Singh, D.K. PCA–based composite drought index for drought assessment in Marathwada region of Maharashtra state, India. *Theor. Appl. Climatol.* **2022**, *149*, 207–220. [CrossRef]
57. Schwartz, C.; Ellenburg, W.L.; Mishra, V.; Mayer, T.; Griffin, R.; Qamer, F.; Matin, M.; Tadesse, T. A Statistical evaluation of earth-observation-based composite drought indices for a localized assessment of agricultural drought in Pakistan. *Int. J. Appl. Earth Obs. Geoinf.* **2022**, *106*, 102646. [CrossRef]

58. Mathbout, S.; Lopez-Bustins, J.A.; Martin-Vide, J.; Bech, J.; Rodrigo, F.S. Spatial and temporal analysis of drought variability at several time scales in Syria during 1961–2012. *Atmos. Res.* **2018**, *200*, 153–168. [CrossRef]
59. Zarei, A.R.; Moghimi, M.M.; Mahmoudi, M.R. Analysis of changes in spatial pattern of drought using RDI index in south of Iran. *Water Resour. Manag.* **2016**, *30*, 3723–3743. [CrossRef]
60. Zarei, A.R.; Moghimi, M.M.; Mahmoudi, M.R. Parametric and non-parametric trend of drought in arid and semi-arid regions using RDI index. *Water Resour. Manag.* **2016**, *30*, 5479–5500. [CrossRef]
61. Sharma, S. *Applied Multivariate Technique*; John Wiley & Sons: New York, NY, USA, 1995.
62. Rencher, A.C. *Multivariate Statistical Inference and Applications*; Wiley: New York, NY, USA, 1998.
63. North, G.R.; Bell, T.L.; Cahalan, R.F.; Moeng, F.J. Sampling errors in the estimation of empirical orthogonal functions. *Mon. Wea. Rev.* **1982**, *110*, 699–706. [CrossRef]
64. Raziei, T.; Saghafian, B.; Paulo, A.A.; Pereira, L.S.; Bordi, I. Spatial patterns and temporal variability of drought in western Iran. *Water Resour. Manag.* **2009**, *23*, 439–455. [CrossRef]
65. Goovaerts, P. *Geostatistics for Natural Resources Evaluation*; Oxford University Press: New York, NY, USA, 1997.
66. Minasny, B.; McBratney, A.B.; Whelan, B.M. *VESPER*, version 1.6; Australian Centre for Precision Agriculture, The University of Sydney: Sydney, NSW, Australia, 2006.
67. Hamed, K.H.; Ramachandra Rao, A. A modified Mann-Kendall trend test for autocorrelated data. *J. Hydrol.* **1998**, *204*, 182–196. [CrossRef]
68. Mann, H.B. Nonparametric tests against trend. *Econometrica* **1945**, *13*, 245–249. [CrossRef]
69. Kendall, M.G. *Rank Correlation Methods*; Charles Griffin: London, UK, 1975.
70. Mitchell, J.M.; Dzerdzeevskii, B.; Flohn, H. *Climate Change*, 79th ed.; World Meteorological Organization: Geneva, Switzerland, 1966.
71. Daufresne, M.; Lengfellner, K.; Sommer, U. Global warming benefits the small in aquatic ecosystems. *Proc. Natl. Acad. Sci. USA* **2009**, *106*, 12788–12793. [CrossRef]
72. Sen, P.K. Estimates of the regression coefficient based on Kendall's tau. *J. Am. Stat. Assoc.* **1968**, *63*, 1379–1389. [CrossRef]
73. Svoboda, M.; LeComte, D.; Hayes, M.; Heim, R.; Gleason, K.; Angel, J.; Rippey, B.; Tinker, R.; Palecki, M.; Stooksbury, D.; et al. The drought monitor. *B Am. Meteorol. Soc.* **2002**, *83*, 1181–1190. [CrossRef]
74. Lloyd-Hughes, B.; Saunders, M.A. A Drought Climatology for Europe. *Int. J. Climatol.* **2002**, *22*, 1571–1592. [CrossRef]
75. Dai, A. Characteristics and trends in various forms of the Palmer Drought Severity Index during 1900–2008. *J. Geophys. Res.* **2011**, *116*, D12115. [CrossRef]
76. Taibi, S.; Meddi, M.; Souag-Gamane, D.; Mahe, G. Évolution et régionalisation des précipitations au nord de l'Algérie (1936–2009). *IAHS* **2013**, *359*, 191–197.
77. Bessaklia, H.; Serrano-Notivoli, R.; Ghenim, A.N.; Chikh, H.A.; Megnounif, A. Extreme precipitation trends in northeast Algeria using a high-resolution gridded daily dataset. *Int. J. Climatol.* **2021**, *41*, 6573–6588. [CrossRef]
78. Mrad, D.; Dairi, S.; Boukhari, S.; Djebbar, Y. Applied Multivariate analysis on annual rainfall in the northeast of Algeria. *J. Water Clim. Change* **2020**, *11*, 1165–1176. [CrossRef]
79. Zerouali, B.; Chettih, M.; Abda, Z.; Mesbah, M.; Santos, C.A.G.; Brasil Neto, R.M. A new regionalization of rainfall patterns based on wavelet transform information and hierarchical cluster analysis in northeastern Algeria. *Theor. Appl. Climatol.* **2022**, *147*, 1489–1510. [CrossRef]
80. Di Lena, B.; Vergni, L.; Antenucci, F.; Todisco, F.; Mannocchi, F. Analysis of drought in the region of Abruzzo (Central Italy) by the standardized precipitation index. *Theor. Appl. Clim.* **2014**, *115*, 41–52. [CrossRef]
81. Mathbout, S.; Lopez-Bustins, J.A.; Royé, D.; Martin-Vide, J. Mediterranean-scale drought: Regional datasets for exceptional meteorological drought events during 1975–2019. *Atmosphere* **2021**, *12*, 941. [CrossRef]